Journal of Solid State Chemistry 184 (2011) 3216–3220

Contents lists available at SciVerse ScienceDirect

Journal of Solid State Chemistry

journal homepage: www.elsevier.com/locate/jssc

Magnetic and electronic properties of nanocrystalline $Gd_3Fe_5O_{12}$ garnet

H. Lassri [a], E.K. Hlil [b,*], S. Prasad [c], R. Krishnan [d]

[a] LPMMAT, Université Hassan II-Ain Chock, Faculté des Sciences, B.P. 5366, Mâarif, Casablanca, Morocco
[b] Institut Néel, CNRS et Université Joseph Fourier, BP 166, F-38042, Grenoble cedex 9, France
[c] Department of Physics, Indian Institute of Technology Bombay, Powai, Mumbai 400076, India
[d] Groupe d'étude de la Matière Condensée, CNRS/Université de Versailles-St-Quentin, 45, avenue des Etats-Unis, 78035 Versailles Cedex, France

ARTICLE INFO

Article history:
Received 23 May 2011
Received in revised form
26 September 2011
Accepted 28 September 2011
Available online 6 October 2011

Keywords:
Nanocrystalline garnet
Magnetization
Local random anisotropy
DOS
Moment magnetic
Spin density

ABSTRACT

The $Gd_3Fe_5O_{12}$ nanocrystalline Gadolinium Iron Garnet (GdIG) obtained from a sintered block was milled in a high energy ball mill. We measured the magnetization at 5 K under applied fields up to 12 T. We report here our study of approach to saturation magnetization. The results have been interpreted within the framework of random anisotropy model. From an analysis of the approach to saturation magnetization some fundamental parameters have been extracted. We have determined the anisotropy field H_r and the local magnetic anisotropy constant K_L. In addition, first-principles spin-density functional calculations, using the Full potential Linear Augmented Plane Waves (FLAPW) method are performed to investigate electronic and magnetic structures. All computed parameters are discussed and compared to available experimental data.

1. Introduction

Nanocrystalline magnetic materials are being currently studied in several laboratories. One of them is the ferromagnetic oxides, such as the spinels and garnets. These oxide materials are attractive for certain applications in the microwave region hence much attention is being given to them. There are essentially two types of nanomaterials that are being studied, namely, the nanopowder obtained by power ball milling of the bulk sintered materials and thin films prepared either by sputtering or by pulsed laser deposition techniques. There is a plethora of publications on such materials dealing with the preparation and study of their magnetic properties [1–3]. The properties of the nanomaterials are found to be different from their bulk counterpart. It is generally observed that for nanomaterials both magnetization and the Curie temperature show a decrease. However in some cases novel behaviour is found. For instance, reduction in grain size leads also to changes in the cation distribution, magnetization and Néel temperature [4,5]. As regards garnets the results are somewhat surprising. Both $Y_3Fe_5O_{12}$ Yttrium iron (YIG) and $Gd_3Fe_5O_{12}$ Gadolinium iron garnets (GdIG) when ball milled to produce nanocrystalline material, below a certain critical size, showed a phase decomposition resulting in the formation of orthoferrite [6]. We have reported in detail our study on nanocrystalline GdIG and also discussed the magnetic properties [7]. Besides such changes, there is a common behaviour in most of the nanospinels and garnets both as thin films and nanopowders that is the difficulty to attain magnetic saturation. In their bulk state these materials which are cubic could be saturated with moderate applied fields of the order of 0.5 T, whereas in their nanostate, they do not show saturation even at 2 T. This has been reported by many authors working on nanograin ferrites who invoke several models to explain the small but definite positive slope in the M–H curve near the saturation point [8,9]. This slope is termed as high field susceptibility and some authors have analysed this to some extent.

In this paper, the anisotropy in nanocrystalline $Gd_3Fe_5O_{12}$ garnet is calculated and discussed. Fundamental parameters of such nanocrystalline are estimated as well. In addition, electronic and magnetic structures calculations, using the FLAPW method, are reported.

2. Experimental

Gadolinium iron garnet obtained from a sintered block was milled in air in a Fritsch P7 high energy ball milling using zirconia balls and vial. The ball to powder weight ratio was 10:1. The magnetic measurements were performed using a quantum design SQUID magnetometer for fields up to12 T at 5 K. X-ray diffraction (XRD) measurements were carried out using a Fe target. The average grain size D was calculated from the XRD measurements using the Scherrer formula.

* Corresponding author.
E-mail address: hlil@grenoble.cnrs.fr (E.K. Hlil).

0022-4596/$ - see front matter © 2011 Elsevier Inc. All rights reserved.
doi:10.1016/j.jssc.2011.09.034

3. Electronic structure calculations

We used the FLAPW method [10] which performs the density functional theory (DFT) calculations using the General Gradient Approximation (GGA) where the Kohn–Sham equation and energy functional are evaluated self-consistently. For this method, the space is divided into the interstitial region and the non-overlapping muffin tin spheres centred on the atomic site. The employed basis function inside each atomic sphere is a linear expansion of the radial solution of a spherically potential multiplied by spherical harmonics. In the interstitial region the wave function is taken as an expansion of plane waves and no shape approximation for the potential is introduced in this region; which is consistent with the full potential method convenient to nonmetallic compounds. The core electrons are described by atomic wave functions which are solved fully relativistically using the current spherical function base and the valence electrons are treated with the spin polarized potential in our case.

The crystallographic structure as reported in Ref. [11] is defined in the space group *Ia*-3*d* (#230) with 4 independent atoms: gadolinium, oxygen and the two iron atoms successively at 24*c*, 96*h*, 16*a* (octahedral) and 24*d* (tetrahedral) sites. The GdIG material is considered to be in the collinear magnetic state where the magnetic moments of octahedral and tetrahedral sites are opposite. The atomic muffin-tin (MT) spheres, supposed not to overlap with each other, are taken as 2.26, 1.8, and 1.6 a.u for Gd, Fe and O, respectively. The gap energy, which defines the separation of the valence and core state, was chosen equal to -6.0 Ry. The largest reciprocal vector G in the charge Fourier expansion, G_{max}, was equal to 14 and the cut-off energy corresponding to the product of the muffin-tin radius and the maximum reciprocal space vector, $R_{MT} \times k_{max}$, was equal to 7. Inside the atomics spheres, the potential and charge density are expanded in crystal harmonics up to $l_{max}=10$. Calculations are performed with 20 inequivalent k-points in the irreducible Brillouin. Such value is sufficiently large to ensure the spin–spin moment. The convergence criterion was chosen to be the total energy and set at 10^{-4} eV.

4. Results and discussion

Fig. 1 shows the XRD pattern of the as-prepared and 10 h milled samples. The 10 h milled sample shows the decomposition of the garnet phase to gadolinium orthoferrite and Gd_2O_3. The average grain size for the as-prepared and 10 h milled samples is 78 and 33 nm, respectively. Fig. 2 shows the field dependence of magnetization at 5 K for the as-prepared and 10 h milled samples. The magnetization at 5 K decreases with milling, due to increase in the

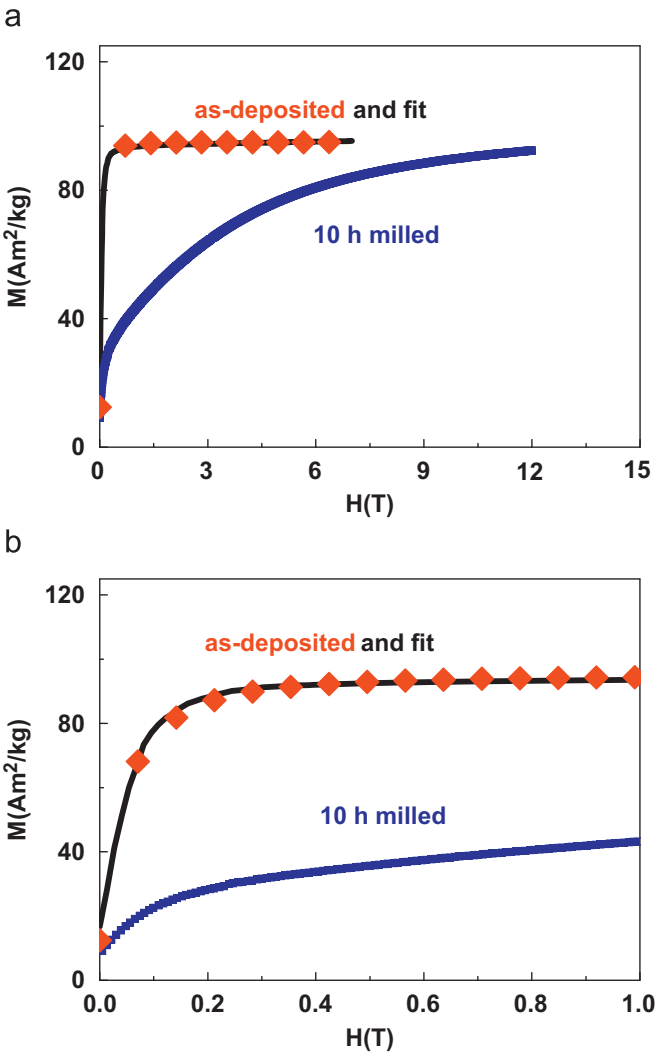

Fig. 2. Experimental curve of $M(H)$ for the as deposited and 10 h milled GdIG samples at 5 K and the fit by the model used. (a) H varies from 0 to 12 T and (b) H varies from 0 to 1 T.

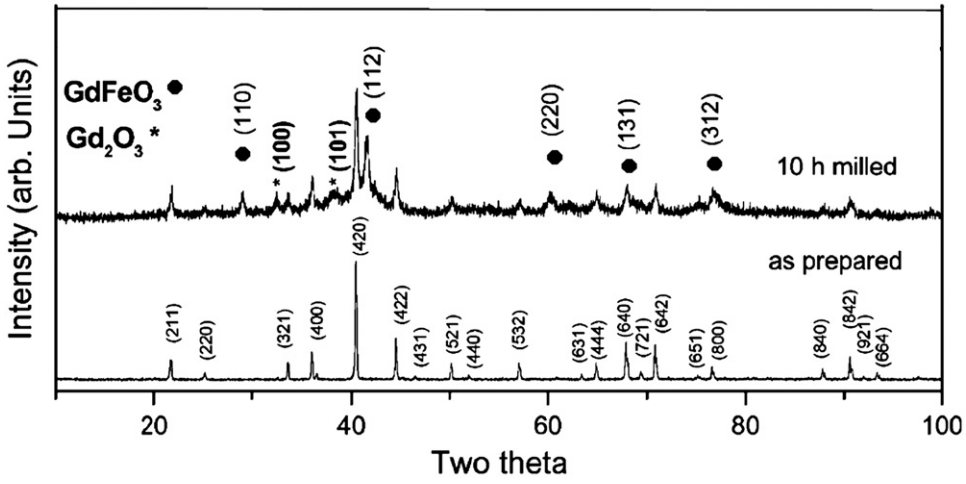

Fig. 1. XRD spectrum for the as deposited and 10 h milled GdIG samples. The symbols indicate the positions of $GdFeO_3$ and Gd_2O_3.

volume fraction of the antiferromagnetic oxides and nonmagnetic phases on milling as revealed by XRD. The magnetic saturation for 10 h milled sample is not reached even with an applied field of 12 T whereas the saturation is easily obtained at a smaller field of 0.7 T for the as-prepared sample. We attribute this difficulty to attain saturation to the presence of the canted spin structure in the milled sample. The canted spin structure could arise due to the presence of multiple magnetic phases and the $M(H)$ curve cannot be fitted with a random anisotropy model. Here we discuss only the approach to saturation for the as-prepared sample where the grain size has been calculated to be 78 nm. It should be noticed that for such nanograins the spin glass effect is excluded as reported by Phan et al. in their magnetocaloric effect investigation on nanocrystalline $Gd_3Fe_5O_{12}$ garnet [12].

Random magnetic anisotropy (RMA) was first proposed by Harris and Plischke [13] to explain the anisotropy found in some amorphous alloys and particularly those containing rare earth metals. They attributed this anisotropy to the topological disorder. The random anisotropy according to this model arises out of crystal field effects of local sites. Since there is a topological disorder the symmetry axes of the sites are oriented at random. Thus there is no single direction of either easy or hard axis. These axes are spread in all directions making it difficult to saturate.

Based on their Hamiltonian, Chudnovsky [14–16] proposed a model to analyse the approach to saturation. This model was applied successfully to explain the results by several authors. We had used this model to analyse our results on several rare earth based amorphous alloys and obtained various fundamental parameters such as local anisotropy, the correlation lengths, etc. [17]. We propose to apply similar ideas to the nanomaterials.

The application of this random anisotropy model to nanomaterials could be justified as follows. The nanograins due to their low dimension have a lower symmetry in the regions particularly near the surface, resulting in a kind of uniaxial anisotropy. As the grains are oriented at random there is no alignment of this axis which then leads to a spread in their direction. This is then analogous to the amorphous materials where the topological disorder leads to a spread in the axis of symmetry. The essential difference of course is that in the amorphous alloys the structural correlation length is of the order of 1 or 2 nm whereas in nanomaterials the grains size is an order of magnitude bigger. This would result in some differences in details and could affect the magnitude of the anisotropy. We briefly describe below the model we have used. We can describe the approach to magnetic saturation by the formula [14–17]

$$M(H) = M_0\left(1-\frac{a_2}{(H+H_u+H_{ex})^2}\right), \quad (1)$$

$$a_2 = \frac{H_r^2}{15} = \frac{1}{15}\left(\frac{2K_L}{M_0}\right)^2, \quad (2)$$

where H is the applied magnetic field in (T), M_0 is the saturation magnetization in Am^2/kg, H_U is the coherent anisotropy field, H_{ex} is the exchange field and a_2 is a constant which is a function of K_L the local anisotropy and M_0. From the best fit, values of M_0, and a_2 were obtained and subsequently were used to determine K_L using Eq. (2). Values of the parameters obtained by this way are displayed in Table 1. In nanocrystalline GdIG, the anisotropy constant calculated from the law of approach to saturation is 10^5 J/m^3. This value of anisotropy is much higher than 2.2×10^4 J/m^3 found for a bulk crystal GdIG. The observation of such high anisotropies in nanocrystalline garnet is surprising in view of fact that the Fe and Gd ions can be regarded as purely S-state ions. It suggests the presence of the dipolar interaction and the single-ion anisotropy.

Total density of state (DOS) deduced from the band structure calculations for $Gd_3Fe_5O_{12}$ is presented in Fig. 3. The main

Table 1
values of the saturation magnetisation M_0, the coefficient a_2, the fields $H_{ex}+H_r$ and K_L for as-prepared sample at 5 K obtained from the fit.

M_0 (Am^2/kg)	a_2 (T^2)	H_U+H_{ex} (T)	H_r (T)	K_L (J/m^3)
95 (16 μ_B/f.u.)	76.8×10^{-4}	932×10^{-4}	3394×10^{-4}	10^5

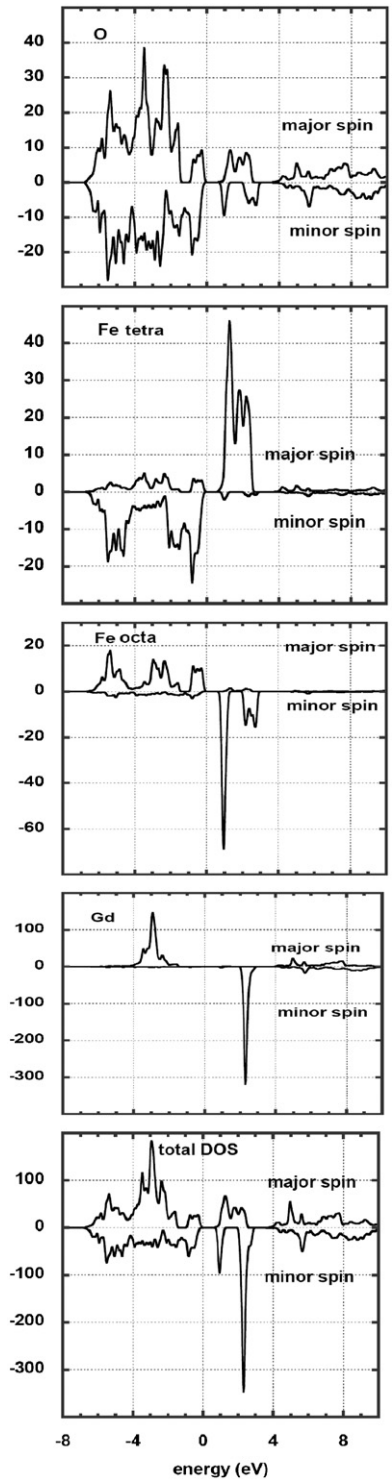

Fig. 3. Total and partials GdIG density of states (for spin up and down) showing the not electric conductor character of GdIG. The Fermi energy is located for Energy=0. Fe_{octa} and Fe_{tetra} denote respectively the octahedral and tetrahedral iron sites.

evidence is the presence of the Fermi level E_F (taken as energy reference) within gap confirming the insulator character of this compound. In addition, the difference in the DOS shape for spin up and spin down confirms the magnetic state as expected. The above results fit with the traditionally picture of the magnetism of insulator compounds.

Details analysis of Gd DOS point out that total DOS is dominated by Gd contributions and show that the fully 4-*f* spin up and empty 4-*f* *spin down* of Gd atom contribute to both occupied states (at −3 eV) and unoccupied sates (at 2.3 eV). Such observed splitting, as known, is induced by higher exchange spin in Gd 4-*f* band since $S=7/2$. Analysis of Fe DOS gives evidence that Fe on tetrahedral site and Fe on tetrahedral site are in antiferromagnetic state while Gd orders ferromagnetically with Fe on octahedral site. Small difference between major spin and minor spin is observed on Oxygen DOS which can be explained in terms of DOS polarisation induced by the presence of small magnetic moment on oxygen atoms.

Magnetic moments carried by atoms are computed as well. Table 2 gathers the resulting magnetic moments as deduced from the differences between the spin up and spin down populations of electron in each atomic sphere and in the interstitial region. Magnetic moment localized on atoms are 6.85 μ_B, −0.08 μ_B, −3.45 μ_B and 3.57 μ_B, which are values as expected in this material type. Computed magnetization of 16 μ_B/f.u. agrees with our experimental data from Table 1. It is worthy noticed that such integer value points out also to insulator state of our material since for insulating systems the magnetic moments are considered as integer values. As surprising additional evidence, we found −0.87 μ_B as a value of interstitial magnetism. Such substantial interstitial magnetism clearly reveals the existence of a noticeable spin density out of iron atomic. Taking into account the electrical insulator character of the GdIG as confirmed by the total density of state and computed magnetization, we expect that the spin density is localized in some well defined region in the crystallographic structure not previously fixed by a particular model. For this aim, we are interested in the spin density calculations. After convergence of the self-consistent process based on FLAPW calculations, the difference between the major spin and minor spin electronic density is performed and 3D as well as 2D maps are built using Xcrysden program [18] and displayed in Figs. 4 and 5, respectively. By examination of 3D spin density map built in primitive unit cell seen in Fig. 4, it could be deduced that the spin density takes the form of the dual polyhedral of the coordination ones. Indeed, the octahedral iron atom presents a spin distribution in form of rounded cube while the tetrahedral iron shows a rounded tetrahedral distribution. These spin distributions can be explained as the 3*d* electrons avoid the oxygen atoms.

We also analyzed the oxygen spin density. As seen in Fig. 5, the shape of spin density on the oxygen atoms exhibits a quadrupolar spin distribution with the positive (in red) and negative (in blue) parts (see yellow arrow). On the other hand, the oxygen spin distribution is very anisotropic and presents a net magnetic quadrupolar feature.

Table 2
Magnetic moments from FLAPW calculations for Gd, Oxygen, Fe on tetrahedral site, Fe on octahedral site, interstitial region and total magnetic moment in $Gd_3Fe_5O_{12}$.

Gd (μ_B)	O (μ_B)	Fe_{tetra} (μ_B)	Fe_{octa} (μ_B)	Interstitial region (μ_B)	Magnetization (μ_B/f.u.)
6.85	0.08	−3.45	+3.57	−0.87	16

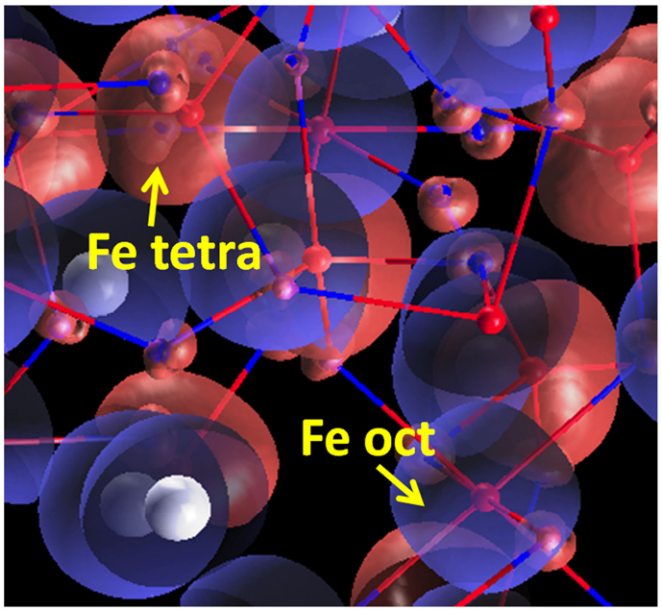

Fig. 4. Perspective view showing the unlocalized spin density on Fe sites. The dual coordination polyhedron form of the spin densities on the octahedral (dual cube) and tetrahedral (dual tetrahedron) are clearly evidenced.

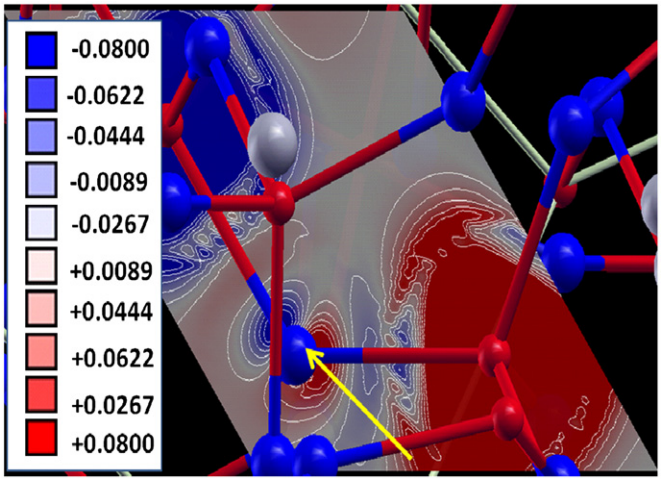

Fig. 5. Perspective view displaying the spin density in the plane Fe_{oct}–O–Fe_{tetra} in $Gd_3Fe_5O_{12}$. We can see form of spin density on the oxygen atoms that exhibits a quadrupolar spin distribution with the positive (in red) and negative (in blue) parts (yellow arrows). (For interpretation of the references to colour in this figure legend, the reader is referred to the web version of this article.)

5. Conclusion

We have shown that it is possible to extend the application of random magnetic anisotropy model originally developed for amorphous alloys to the nanocrystalline materials gadolinium iron garnet. The model gives a good fit of the experimental $M(H)$. In addition, we have determined some fundamental parameters such as random anisotropy fields and random anisotropy constant. We find that the local anisotropy is at least an order of magnitude higher than in the corresponding bulk garnet. First-principles spin-density functional calculations, using FLAPW method, are performed to probe magnetic structure details. Namely, magnetic moments carried by atoms are computed and magnetization is found equal to experimental data. Moreover, substantial interstitial magnetism is revealed and the oxygen spin

distribution is found very anisotropic and presents a net magnetic quadrupolar feature.

References

[1] E. Popova, N. Keller, F. Gendron, M. Guyot, M.-C. Brianso, Y. Domond, M. Tessier, J. Appl. Phys. 90 (2001) 1422.
[2] J.H. Yin, J. Ding, J.S. Chen, X.S. Miao, J. Magn. Magn. Mater. 303 (2006) e387.
[3] M. Bohra, S. Prasad, N. Kumar, D.S. Misra, S.C. Sahoo, N. Venkataramani, R. Krishnan, Appl. Phys. Lett. 88 (2006) 262506.
[4] C.N. Chinnasamy, A. Narayanasamy, N. Ponpandian, K. Chattopadhyay, H. Guerault, J.M. Greneche, J. Phys. Condens. Matter 12 (2000) 7795.
[5] C.N. Chinnasamy, A. Narayanasamy, N. Ponpandian, K. Chattopadhyay, K. Shinoda, B. Jeyadevan, K. Tohji, K. Nakatsuka, T. Furubayashi, I. Nakatani, Phys. Rev. B 63 (2001) 184108.
[6] R.J. Joseyphus, A. Narayanasamy, N. sivakumar, M. Guyot, R. Krishnan, N. Ponandian, K. Chattopadhay, J. Magn. Magn. Mater. 238 (2002) 281.
[7] R.J. Joeseyphus, A. Narayanasamy, A.K. Nigam, R. Krishnan, J. Magn. Magn. Mater. 296 (2006) 57.
[8] D.T. Margulies, F.T. Parker, A.E. Berkowitz, J. Appl. Phys. 75 (1994) 6097.
[9] J. Dash, S. Prasad, N. Venkataramani, R. Krishnan, P. Kishan, N. Kumar, S.D. Kulkarni, S.K. Date, J. Appl. Phys. 86 (1999) 3303.
[10] P. Blaha, K. Schwartz, P. Sorantin, S.B. Trikey, Comput. Phys. Common. 59 (1990) 399.
[11] J.E. Weidenborner, Acta Cryst. 14 (1961) 1051.
[12] M.H. Phan, M.B. Morales, C.N. Chinnasamy, B. Latha, V.G. Harris, H. Srikanth, J. Phys. D: Appl. Phys 42 (2009) 115007.
[13] R. Harris, M. Plichke, M.J. Zuckerman, Phys. Rev. Lett. 31 (1973) 160.
[14] E.M. Chudnovsky, W.M. Saslow, R.A. Serota, Phys. Rev. B 33 (1986) 251.
[15] E.M. Chudnovsky, J. Appl. Phys. 64 (1988) 5770.
[16] E.M. Chudnovsky, J. Magn. Magn. Mater. 79 (1989) 127.
[17] H. Lassri, R. Krishnan, J. Magn. Magn. Mater. 104–107 (1992) 157.
[18] Kokalj, Comput. Mater. Sci. 28 (2003) 155.